Saeedifar, Milad and Najafabadi, Mehdi Ahmadi and Zarouchas, Dimitrios and Toudeshky, Hossein Hosseini and Jalalvand, Meisam (2018) Clustering of interlaminar and intralaminar damages in laminated composites under indentation loading using acoustic emission. Composites Part B: Engineering, 144. pp. 206-219. ISSN 1359-8368 , http://dx.doi.org/10.1016/j.compositesb.2018.02.028

This version is available at https://strathprints.strath.ac.uk/63781/

Strathprints is designed to allow users to access the research output of the University of Strathclyde. Unless otherwise explicitly stated on the manuscript, Copyright © and Moral Rights for the papers on this site are retained by the individual authors and/or other copyright owners. Please check the manuscript for details of any other licences that may have been applied. You may not engage in further distribution of the material for any profitmaking activities or any commercial gain. You may freely distribute both the url (https://strathprints.strath.ac.uk/) and the content of this paper for research or private study, educational, or not-for-profit purposes without prior permission or charge.

Any correspondence concerning this service should be sent to the Strathprints administrator: strathprints@strath.ac.uk

The Strathprints institutional repository (https://strathprints.strath.ac.uk) is a digital archive of University of Strathclyde research outputs. It has been developed to disseminate open access research outputs, expose data about those outputs, and enable the management and persistent access to Strathclyde's intellectual output.

Clustering of Interlaminar and Intralaminar damages in Laminated Composites under Indentation Loading using Acoustic Emission

Milad Saeedifar[1], Mehdi Ahmadi Najafabadi[*1], Dimitrios Zarouchas[2], Hossein Hosseini Toudeshky[3], Meisam Jalalvand[4,5]

1. Non-destructive Testing Lab, Department of Mechanical Engineering, Amirkabir University of Technology, 424 Hafez Ave, 15914, Tehran, Iran.
2. Structural Integrity & Composites Group, Faculty of Aerospace Engineering, Delft University of Technology, The Netherlands.
3. Department of Aerospace Engineering, Amirkabir University of Technology, 424 Hafez Ave, 15914, Tehran, Iran.
4. Department of Mechanical and Aerospace Engineering, The University of Strathclyde, 75 Montrose Street, Glasgow G1 1XJ, UK
5. Advanced Composites Centre for Innovation and Science, University of Bristol, Bristol BS8 1TR, UK

Abstract

This study focuses on the clustering of the indentation-induced interlaminar and intralaminar damages in carbon/epoxy laminated composites using Acoustic Emission (AE) technique. Two quasi-isotropic specimens with layups of $[60/0/-60]_{4S}$ (is named dispersed specimen) and $[60_4/0_4/-60_4]_S$ (is named blocked specimen) were fabricated and subjected to a quasi-static indentation loading. The mechanical data, digital camera and ultrasonic C-scan images of the damaged specimens showed different damage evolution behaviors for the blocked and dispersed specimens. Then, the AE signals of the specimens were clustered for tracking the evolution behavior of different damage mechanisms. In order to select a reliable clustering method, the performance of six different clustering methods consisting of k-Means, Genetic k-Means, Fuzzy C-Means, Self-Organizing Map (SOM), Gaussian Mixture Model (GMM), and hierarchical model were compared. The results illustrated that hierarchical model has the best performance in clustering of AE signals. Finally, the evolution behavior of each damage mechanism was investigated by the

[*] Corresponding author. Tel.: +98 21 6454 3431; fax: +98 21 8871 2838. E-mail address: ahmadin@aut.ac.ir (M. Ahmadi Najafabadi)

clustered AE signals with hierarchical model. The results of this study show that using AE technique with an appropriate clustering method such as hierarchical model could be an applicable tool for structural health monitoring of composite structures.

Keywords: Acoustic Emission; Laminated Composites; Damage Mechanisms; Clustering Methods; Indentation Loading.

1. Introduction

Carbon Fiber Reinforced Polymer (CFRP) composites are increasingly utilized in many industries due to their high specific strength and stiffness [1-3]. One of the important issues that affected the functionality of these materials is their high susceptibility to damage under out-of-plane loading. This type of load can induce different kinds of interlaminar and intralaminar damages in the composite structure such as delamination, matrix cracking, and fiber failure [4-6]. It will be more critical when the damages occur inside the structure without any evidence on the structure surface [7]. However, the adverse effects of these damage mechanisms on the structural integrity of the composite structures are not equal. For example, delamination reduces the stiffness of the structure considerably while the matrix cracking does not have a significant effect on the stiffness of the composite structures individually. Knowing some information about the type and also amount of the different damage mechanisms in a damaged composite structures is necessary to damage tolerance analysis of the structure. Thus, using a practical method to detect and classify different damage mechanisms in a composite structure is a valuable tool to damage tolerance analysis.

Structural Health Monitoring (SHM) has attracted many attentions to itself during the last decades [8, 9]. Non-Destructive Evaluation (NDE) techniques are capable tools for examining the integrity of laminated composite structures [10-12]. Among the NDE techniques, Acoustic

Emission (AE) is widely utilized for health monitoring of the composite structures [13-18]. AE is defined as the propagation of a transient elastic wave within the material caused by a sudden release of strain energy which can be due to the occurrence of a damage [19]. Detecting, analyzing and clustering of the originated AE signals from a damaged structure lead to obtaining some valuable information about the damage such as the damage location, damage type, amount of damage, etc. Ai et al. [20] used b-value method to analyze the AE signals of carbon/epoxy specimens under three-point bending test. The b-value parameter is an indicator that shows the state of damage in the material. They tracked the evolution of different damage mechanisms in the specimens by this method. Fotouhi et al. [21] classified damage mechanisms in glass/epoxy composites using analyzing of AE signals by Fuzzy C-Means (FCM) clustering. They partitioned three different damages, i.e. matrix cracking, fiber breakage, and fiber/matrix debonding. Pashmforoush et al. [22-23] used Genetic k-Means algorithm to cluster AE signals of the damage mechanisms in glass/epoxy and sandwich laminates under three-point bending and mode I loading conditions. As will be mentioned in the next sections, the drawback of these works is that the performance of FCM and Genetic k-Means methods to data clustering dependents on the selecting of the initial cluster centers and they often get stuck in local minima. Thus, it seems that these methods are not appropriate tools to create a robust and reliable SHM system based on AE technique.

By literature review, it is found that there are many studies on the numerical, analytical, and experimental investigation of the damage mechanisms in laminated composites under indentation and low-velocity impact loadings [24-29]. However, there is only a few research on AE-based study of the indentation and low-velocity impact-induced damages in laminated composites. Suresh Kumar et al. [30] characterized the indentation damage resistance of hybrid composite laminates using AE monitoring. They used the felicity effect and the sentry function for monitoring

the damage state of the material under repeated indentation loading. However, they did not perform the clustering of damage mechanisms. Boominathan et al. [31] used AE to characterize the effect of temperature on the falling weight impact damage in carbon/epoxy laminates. They did not directly analyze the impact-induced damages and instead, the impacted damaged specimens were subjected to the quasi-static flexural loading and the AE behavior of them was studied. Also, they classified AE signals of the specimens based on their frequency content without using any clustering method. Mahdian et al. [32] investigated the indentation-induced damages in glass/epoxy laminated composites by AE. They clustered the damage mechanisms by FCM method. Their study has some drawbacks, one is that the layup of their specimens was unidirectional ($[0_8]$ layup) which is a non-practical layup and therefore no delamination occurred in the specimens. Also, as will be shown in the next sections, FCM clustering is not a reliable and repeatable clustering method to classify the AE signals of the damage mechanisms. Petrucci et al. [33] investigated the effect of hybridization of laminated composites on the impact and post-impact damages. They only used the AE technique to localize the damaged region without any furthermore AE signals analysis.

As been mentioned, there is a lack in AE-based study of indentation and low-velocity impact-induced damages in laminated composites. Also, a few conducted studies on this subject have not used an appropriate clustering method to classify AE signals of damage mechanisms. Therefore, the aim of this study is the clustering of the indentation-induced interlaminar and intralaminar damages in carbon/epoxy laminated composites using AE technique. To achieving the in-plane isotropic properties, most of the real composite structures are fabricated with the quasi-isotropic layup. Also, in order to investigate the effect of ply-thickness on the induced damages, two quasi-isotropic carbon/epoxy laminated composites with $[60/0/-60]_{4S}$ and $[60_4/0_4/-60_4]_S$ layups were fabricated and subjected to a quasi-static indentation loading. The load-displacement results and

the digital camera and ultrasonic C-scan images of the interlaminar and intralaminar damages showed different damage behaviors for the specimens. Then, the AE signals of the damaged specimens were classified to investigate the damage behavior of the specimens. In order to select the best clustering method, the performance of six different clustering methods that mostly have been used in literature consisting of k-Means, Genetic k-Means, FCM, Self-Organizing Map (SOM), Gaussian Mixture Model (GMM), and hierarchical model were compared. Based on the obtained results, the AE signals of the specimens were finally clustered by hierarchical model and the evolution behavior of the different damage mechanisms during indentation loading was studied. The obtained results show that the combination of AE technique with an appropriate clustering method such as hierarchical model can be used as a valuable tool for structural health monitoring of the composite structures.

2. Experimental Procedures

2.1. Description of the Materials

The specimens were fabricated from 24 layers of Hexcel IM7/8552 unidirectional prepregs sheets (from Hexcel® Corporation) curried according to the manufacturer's offered procedure [34]. The physical properties of unidirectional carbon fibers, IM7, and epoxy resin, 8552, and also the mechanical properties of the laminate are represented in Tables 1 and 2.

Table 1. The physical properties of IM7/8552 [34].

Parameter	Value
Fiber density (g/cm^3)	1.77
Resin density (g/cm^3)	1.30
Fiber volume (%)	57.70
Laminate density (g/cm^3)	1.57

Table 2. The mechanical properties of IM7/8552 [35].

E_1 (MPa)	E_2 (MPa)	E_3 (MPa)	ν_{12}	ν_{23}	G_{12} (MPa)	G_{13} (MPa)	G_{23} (MPa)
161000	11400	11400	0.300	0.436	5170	5170	3980

2.2. Test Method

The specifications of the rectangular specimens are presented in Table 3. The quasi-static indentation tests were conducted by forcing a Φ16 mm spherical-head indenter against the specimen which is simply supported over a 125×75 mm^2 hollow window (see Fig. 1). The load was applied under displacement control mode at a constant feed rate of 0.5 mm/min and the temperature of 25°C by an INSTRON servo-hydraulic testing machine. The applied load and vertical displacement were continuously recorded during all the tests by the machine. According to Fig.1, four AE sensors which are placed on the face of the specimen capture the originated AE signals during the tests.

Table 3. The specifications of the specimens.

Specimens	Dimensions (mm)	Lay-up	Ply thickness (mm)
S_D	150×100×3	$[60/0/-60]_{4S}$	0.125
S_B	150×100×3	$[60_4/0_4/-60_4]_S$	0.125

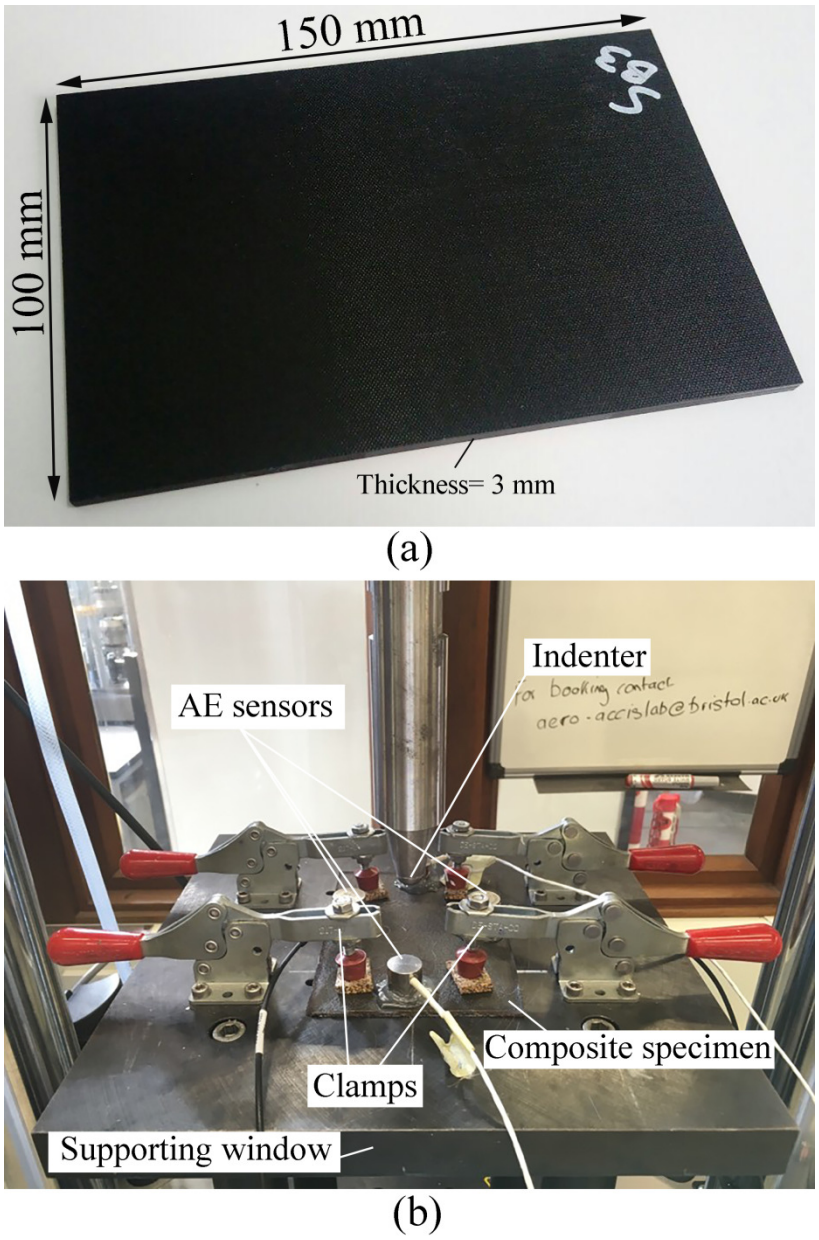

Fig. 1. a) The composite specimen, and b) the indentation test setup.

2.3. AE system

The utilized AE sensors, WD, were broadband, resonant-type, and single-crystal piezoelectric transducers from Physical Acoustics Corporation (PAC). The optimum operating frequency range of the AE sensors was [100–900 kHz]. The AE events were recorded by the AE software, AEWin, and a data acquisition system PAC-PCI-2 with a maximum sampling rate of 40 MHz. Vacuumed

silicon grease was used as the acoustical coupling. The recorded AE signals were enhanced by a 2/4/6-AST preamplifier. The gain selector of the preamplifier and the threshold of receiving AE signals were set to 40 dB. The test-sampling rate was 5 MHz with 16 bits of resolution between 10 and 100 dB. The threshold of receiving AE signals was adjusted to 40 dB. A pencil lead break procedure was used to calibrate the data acquisition system and ensure good conductivity between the specimen surface and the sensors [36]. In order to record the AE signals during the tests, four AE sensors were placed on the front face of the specimens. Then, some features of these signals such as amplitude, frequency, and absolute energy (the integral of the squared voltage signal above the threshold which is divided by a reference resistance over the AE signal duration) were extracted to study the damage state of the specimens.

3. The Proposed Methods

In this section, a brief description of the utilized clustering methods in this study is represented. The aim is partitioning a set of AE signals, $\{A_1, A_2, \cdots, A_n\}$, which each signal has p features, $A_1=[a_1, a_2, \ldots, a_p]$), into k clusters ($k \leq n$), $\{C_1, C_2, \cdots, C_k\}$.

k-Means clustering: k-Means is an iterative clustering method that attempts to partition a set of data so that the sum of distance (similarity) between with-in cluster data to clusters centroid be minimized. The k-Means algorithm consists of two phases [37]:

Assignment phase: Assigns each data to the cluster with the nearest cluster centroid.

$$C_i^{(t)} = \{A_n : \left\| A_n - m_i^{(t)} \right\|^2 \leq \left\| A_n - m_j^{(t)} \right\|^2 \ \ \forall j, 1 \leq j \leq k\} \tag{1}$$

where $C_i^{(t)}$ is cluster i and $m_i^{(t)}$ is the center of cluster i.

Update phase: The centroid of each cluster is recalculated and considered as the mean value of the cluster's member data.

$$m_i^{(t+1)} = \frac{1}{\left|C_i^{(t)}\right|} \sum_{A_j \in C_i^{(t)}} A_j \tag{2}$$

These two phases are iterated until the clusters do not change anymore. There is no guarantee that the algorithm converges to an optimum solution because the performance of the algorithm depends on the initial randomly selected clusters centroid [23, 38].

Genetic k-Means clustering: In order to reduce the probability that k-Means get stuck in local minima, the Genetic algorithm could be linked to k-Means to establish an equilibrium between local exploitation and global exploration. It could lead to finding a near-optimum solution. The details of this algorithm can be found in our previous study [23].

***FCM clustering*:** Although FCM clustering is similar to k-Means, however, they have some differences. The most significant difference is that in FCM clustering, a data point does not definitely belong to only one cluster and it can appertain to some other clusters concurrently, with different values of membership parameter between 0 and 1 [21]. If the membership value of a data point for a cluster is close to 1, this data is closer to that cluster. The FCM attempts to minimize the following objective function [39]:

$$J(A;C) = \sum_{i=1}^{k} \sum_{j=1}^{n} (\gamma_{ij})^{\alpha} \left\| A_j - C_i \right\|^2 \tag{3}$$

$$D_{ij}^2 = \left\| A_j - C_i \right\|^2 = (A_j - C_i)^T (A_j - C_i) \tag{4}$$

As can be seen, this objective function is very similar to the objective function of k-Means with two main differences: addition of membership value (γ_{ij}) and fuzzier (α) that determines the level of fuzziness of the clustering. The objective function will be minimized if [39]:

$$\gamma_{ij} = \frac{1}{\sum_{m=1}^{k} \left(\frac{D_{ij}}{D_{mj}}\right)^{\frac{2}{\alpha-1}}} \quad ; \; 1 \le i \le k, 1 \le j \le n \tag{5}$$

and

$$C_i = \frac{\sum_{j=1}^{n} (\gamma_{ij})^{\alpha} A_j}{\sum_{j=1}^{n} (\gamma_{ij})^{\alpha}} \;\; ; \;\; 1 \le i \le k \tag{6}$$

The FCM algorithm has three phases:

1. Specifying the cluster centers by Eqs. 5 and 6.
2. Calculating the distance by Eq. 4.
3. Updating of the objective function by Eq. 3.

Although the performance of FCM is much better than k-Means, however, it is still possible that FCM gets stuck in local minima, because its performance depends on the selection of the initial cluster centers or/and the initial membership values [40].

SOM clustering: SOM is a type of Neural Networks (NN) that can be trained by an unsupervised learning technique to be utilized as a data partitioning method. In this method, there is a lattice consisting of some neurons with random initial weights. When a data is fed into the network, the similarity of the data with the weight vector of all neurons is checked and finally, the weight vectors of the winning neuron (W_v) and its neighborhood neurons are updated by the following equation [41]:

$$W_v(t+1) = W_v(s) + \theta(u,v,t) \cdot (A_i - W_v(t)) \tag{7}$$

$$\theta(u,v,t) = \exp\left(\frac{\left\| r_u - r_v \right\|^2}{2\sigma^2(t)}\right) \tag{8}$$

where t is the time (step) index, u is the index of the winning neuron for data A_i, $\theta(u,v,t)$ is the neighborhood function which specifies the distance between neuron u and v at step t, r_u and r_v are

the positions of neurons u and v, and $\sigma(t)$ is the width of the neighborhood function. By time proceeding, the SOM lattice gets the shape of the data space and data are clustered.

GMM clustering: GMM is a probabilistic model that assumes the data are a weighted sum of a finite number of Gaussian densities with unknown parameters [42]:

$$p(x) = \sum_{k=1}^{K} w_k g(A|\mu_k, \Sigma_k) \tag{9}$$

$$g(A|\mu_k, \Sigma_k) = \frac{1}{\sqrt{(2\pi)^k |\Sigma_k|}} \exp\left(\frac{-\frac{1}{2}(A-\mu_k)^{\mathrm{T}}}{\Sigma_k (A-\mu_k)}\right) \tag{10}$$

$$\sum_{k=1}^{K} w_k = 1 \tag{11}$$

where A is data, w_k is the mixture weight function, and g is the Gaussian density function with mean vector μ_k and covariance matrix Σ_k.

The GMM algorithm consists of three steps [42]:

1. The algorithm starts with some initial estimation for mean vectors and covariance matrixes. Then, it calculates the weight function for all data and all mixture combinations.
2. Using the membership weight and the data to calculate the new parameters. If the sum of membership weight for k^{th} component is defined as $N_K = \sum w_{ik}$, the new mixture weight can be calculated by:

$$w_k^{new} = \frac{N_k}{N}; \quad 1 \le k \le K \tag{12}$$

The new mean vector and covariance matrix for Gaussian distributions are updated as follows:

$$\mu_k^{new} = (\frac{1}{N_k})\sum_{i=1}^{n} w_{ik} \cdot A_i; \quad 1 \le k \le K \tag{13}$$

$$\Sigma_k^{new} = (\frac{1}{N_k})\sum_{i=1}^{n} w_{ik} \cdot (A_i - \mu_k^{new})(A_i - \mu_k^{new})^{\mathrm{T}}; \quad 1 \le k \le K \tag{14}$$

3. Repeating steps 1 and 2 to satisfy the stopping criterion.

Hierarchical model: Hierarchical model partitions data by creating a cluster tree or dendrogram. This method usually is used under one of two following procedures: 1) divisive, and 2) agglomerative.

Divisive: In this procedure, 4 steps must be passed to achieve an appropriate clustering [43]:

1. Each data is considered as a cluster and the distance between clusters are calculated.
2. Merging of two closest clusters.
3. Calculation of the distance between the new cluster and the previous clusters (The number of clusters has been reduced as one unit)
4. Repeating steps 2 and 3 to achieve the desired clusters number.

Due to the top-down structure of this method, it does not get stuck in local minima.

Agglomerative: It is completely reverse of the divisive approach.

4. Results and Discussions

The results are presented in two sections. At first section, the damage behavior of the specimens is studied based on the mechanical data, the digital camera and ultrasonic C-scan images. At the second section, the AE signals are used to study the damage mechanisms.

4.1. The mechanical data, digital camera and ultrasonic C-scan images

Fig. 2 shows the load-displacement curve of the specimens. The load curve of the specimens have different behaviors. In the first region, where there is a linear relationship between the load and displacement, the flexural rigidity (the slope of the load-displacement curve) of specimen S_D is about 27% higher than specimen S_B which it is consistent with the theoretical calculation result (24%) [44]. The linear part of the curve is extended up to load 3 kN for specimen S_D. It is then followed by a big load drop which is continued by a significant load-carrying recovery up to about 2.6 times of the load magnitude at the first load drop, i.e. 7.8 kN, where, the final failure occurs. The behavior of the load curve of specimen S_B differs from specimen S_D. The linear part of the curve is finished earlier than specimen S_D (i.e. 1.3 kN against 3 kN). In contrast to specimen S_D, the linear part of the load curve of specimen S_B is followed by a smooth reduction of the flexural rigidity without any significant load drop. This nonlinearity is continued up to load 4 kN, where, a big load drop occurs. After this region, there is another load recovery part. The ratio of the maximum load to the load at the end of the linear region is 2.6 and 3.1 for specimens S_D and S_B, respectively. Therefore, the load recycling capability of specimen S_B is higher than specimen S_D. While, based on the resistance against the occurrence of the initial significant damage (the end of the linear region in the load-displacement curve), specimen S_D has a better performance in comparing with specimen S_B (3 kN vs. 1.3 kN). Also, the maximum load of specimen S_D is about 1.7 times of maximum load of specimen S_B.

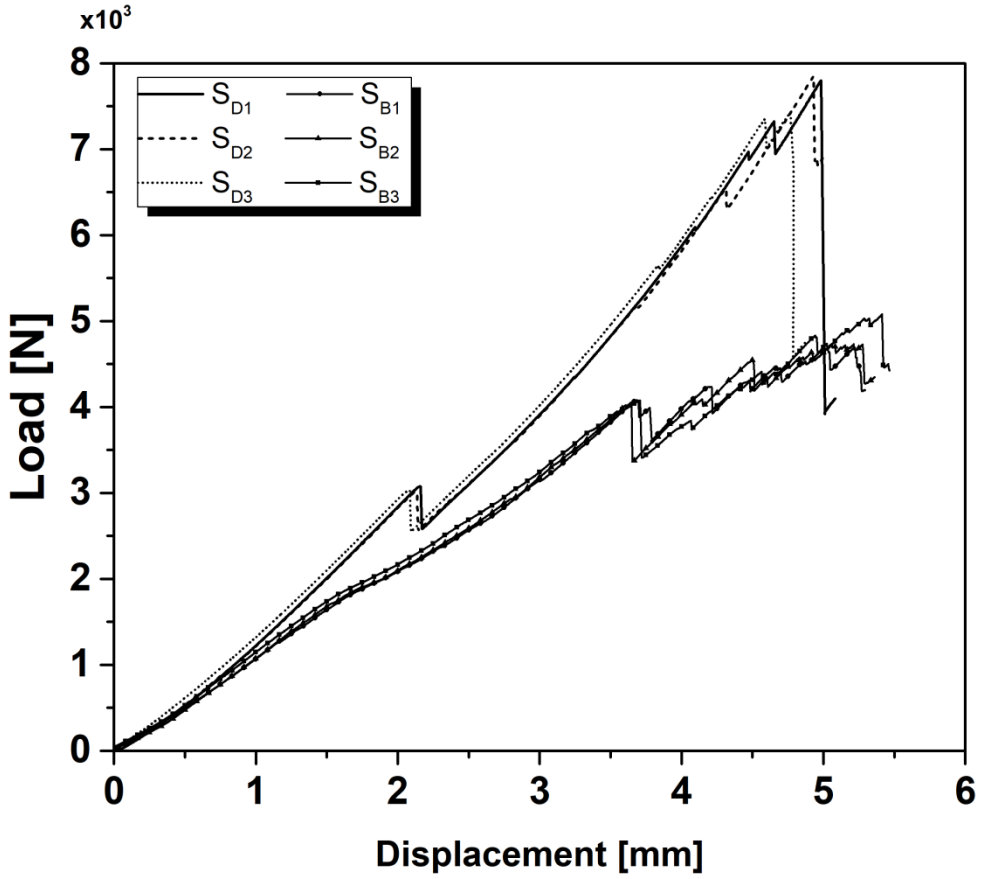

Fig. 2. The load-displacement curve of the specimens.

In order to fully description of the behavior of the damages, in addition to mechanical data, ultrasonic C-scan and digital camera were employed and pictures were taken at different stages of the loading process. To this aim, the state of the interlaminar and intralaminar damages have been studied at three points specified on the load curve as follows (see Fig. 3): point 1 near to the end of the linear elastic region, point 2 just after the linear elastic region, and point 3 at the final failure of the specimens. Fig. 3 shows the digital camera images of the front and back faces of the specimens at these three points. As can be seen, there is no matrix cracking at the first state for both specimens. At the end of the linear elastic region (point 1) some matrix cracking has occurred at the front face of the specimens, just under the punch surface. However, there is no matrix cracking at the back side of the specimens at this point. At point 2, in addition to the front face

matrix cracking, some matrix cracking is observed at the back face of the specimens. At point 3, the size of matrix cracking in the front face does not change significantly but the size of the matrix cracking at the back face obviously has been increased. The damages at the back face of specimen S_D are almost locally and some fiber breakage is even seen, while the damages at the back face of specimen S_B are located inside a wider region and no fiber breakage is also seen. It may show that the dominant loading mode for specimen S_D is penetration, while the dominant loading mode of specimen S_B is bending. As will be explained in the next paragraph, the number of delaminations for specimen S_D is bigger than specimen S_B and the distance between two adjacent delaminations in specimen S_D is also less. Thus, by progressing the loading process and the occurrence of transverse matrix cracks, these delaminations connect to each other and consequently the punch can penetrate to specimen S_D easier than specimen S_B.

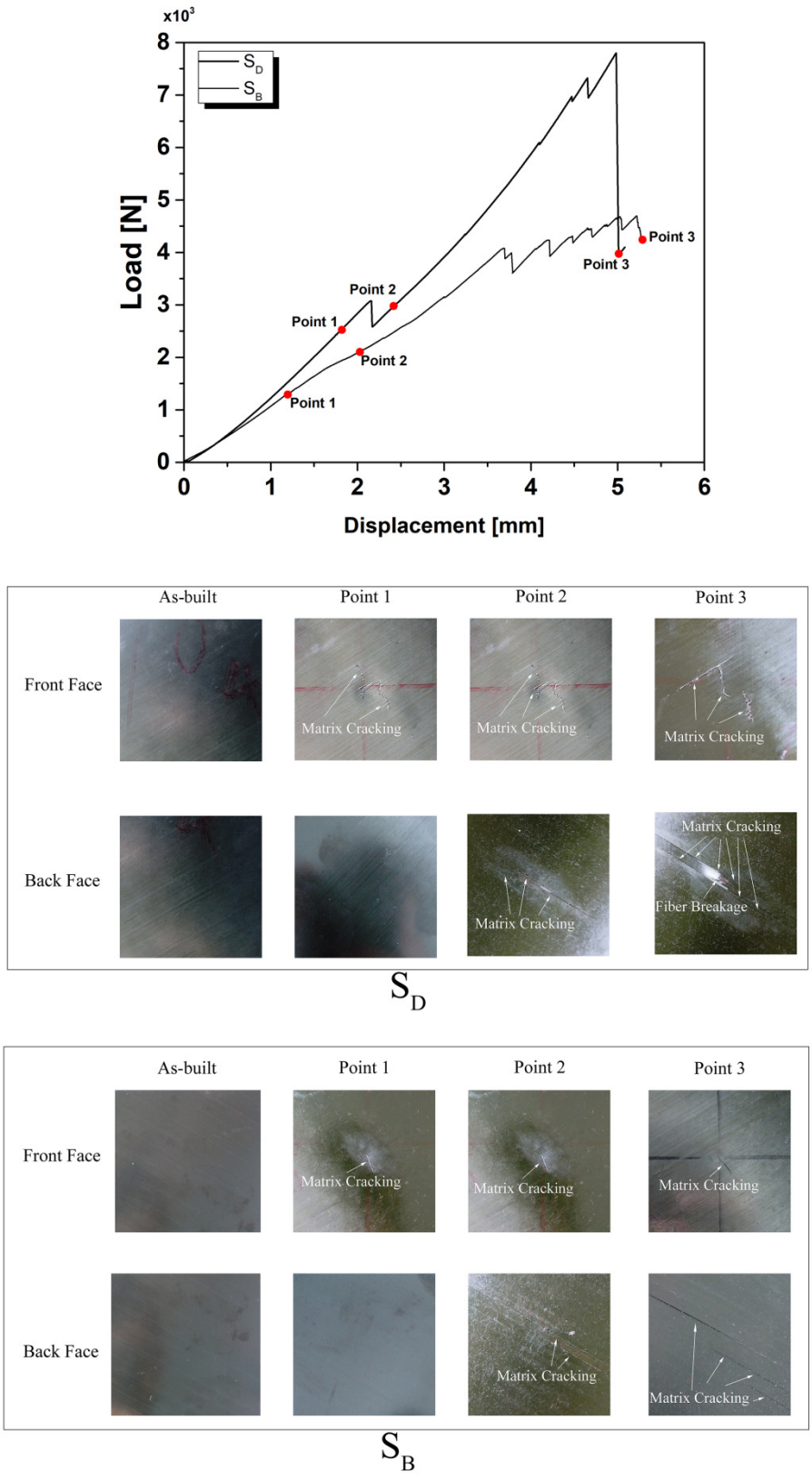

Fig. 3. The damages at the front and back faces of the specimens at different load levels.

Fig. 4 illustrates the detected interlaminar damages in the specimens by the ultrasonic C-scan at points 2 and 3. No delamination was detected by the ultrasonic C-scan at point 1 for both specimens, thus the images of point 1 have not been shown. The C-scan images at point 2 show some delamination. Area of the delaminated region was obtained by calculating area of the delaminated region's pixels by image processing technique and it is reported in Table 4. The area of the delaminated region at point 2 for specimen S_B is 4.5 times of specimen S_D while the number of delaminated interfaces for specimen S_D is higher than specimen S_B. In order to specify the number of delaminated interfaces, some damaged specimens were cutted at the midplane of the longitudinal direction by a cutting machine with a very sharp circular blade. Fig. 5 shows the magnified cross-section overview of the damaged specimens at points 2 and 3. As can be seen, at point 2, at least 7 interfaces of specimen S_D are delaminated while only 2 delaminated interfaces are seen in specimen S_B. The higher number of the delaminated interfaces for specimen S_D is due to the higher number of dissimilar interfaces in this specimen in comparison with specimen S_B (22 dissimilar interfaces for S_D against 4 dissimilar interfaces for S_B). The C-scan images at point 3 show that the area of the delaminated region for specimen S_B gets much bigger than specimen S_D (i.e. 6.9 times), while the number of delaminations for specimen S_D is more than specimen S_B (22 delaminated interfaces for S_D against 4 delaminated interfaces for S_B). The higher area of the delaminated region for specimen S_B in comparison with specimen S_D is due to the higher value of the interfacial shear stress between two adjacent dissimilar plies in this specimen. In other words, the blocking leads to increasing of the interlaminar shear stress at the dissimilar interfaces [45].

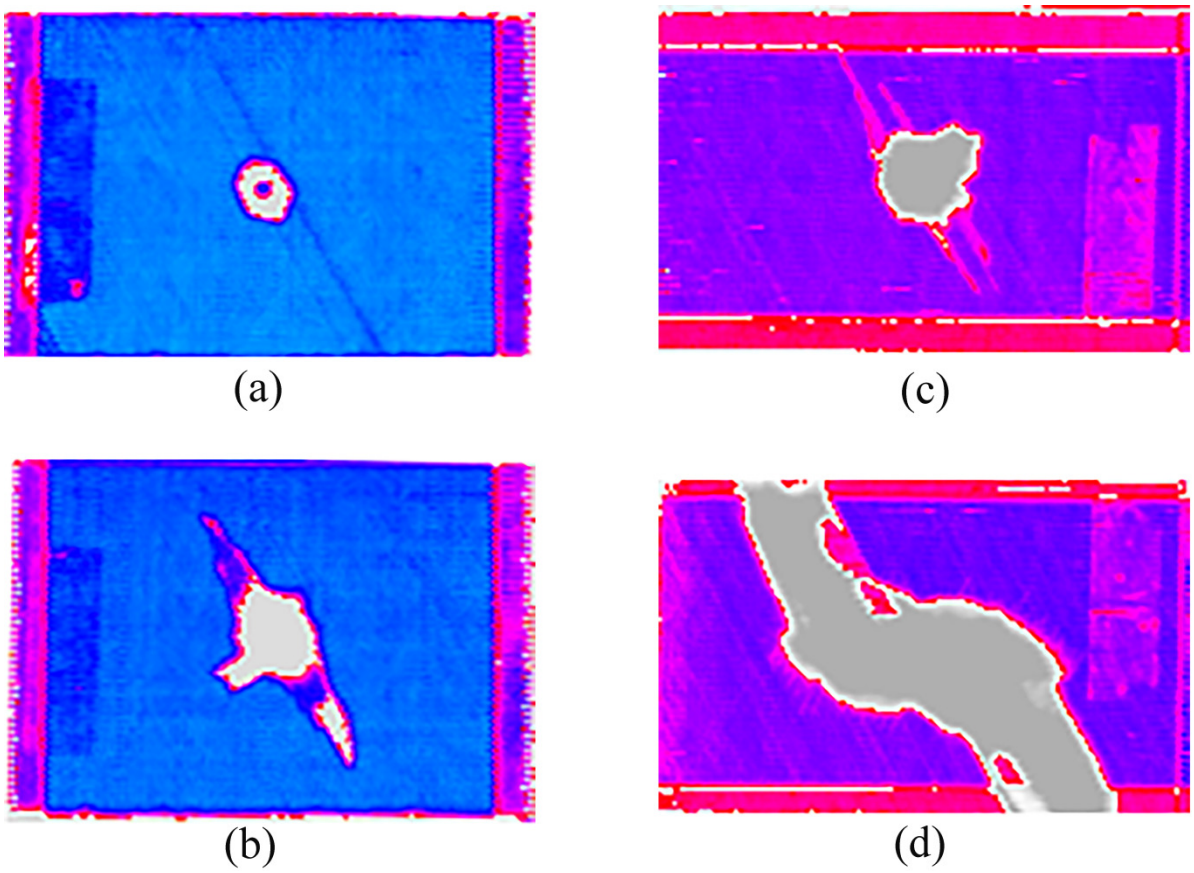

Fig. 4. Delamination contours obtained from ultrasonic C-scan of a) S_D-point 2, b) S_D-point 3, c) S_B-point 2, d) S_B-point 3.

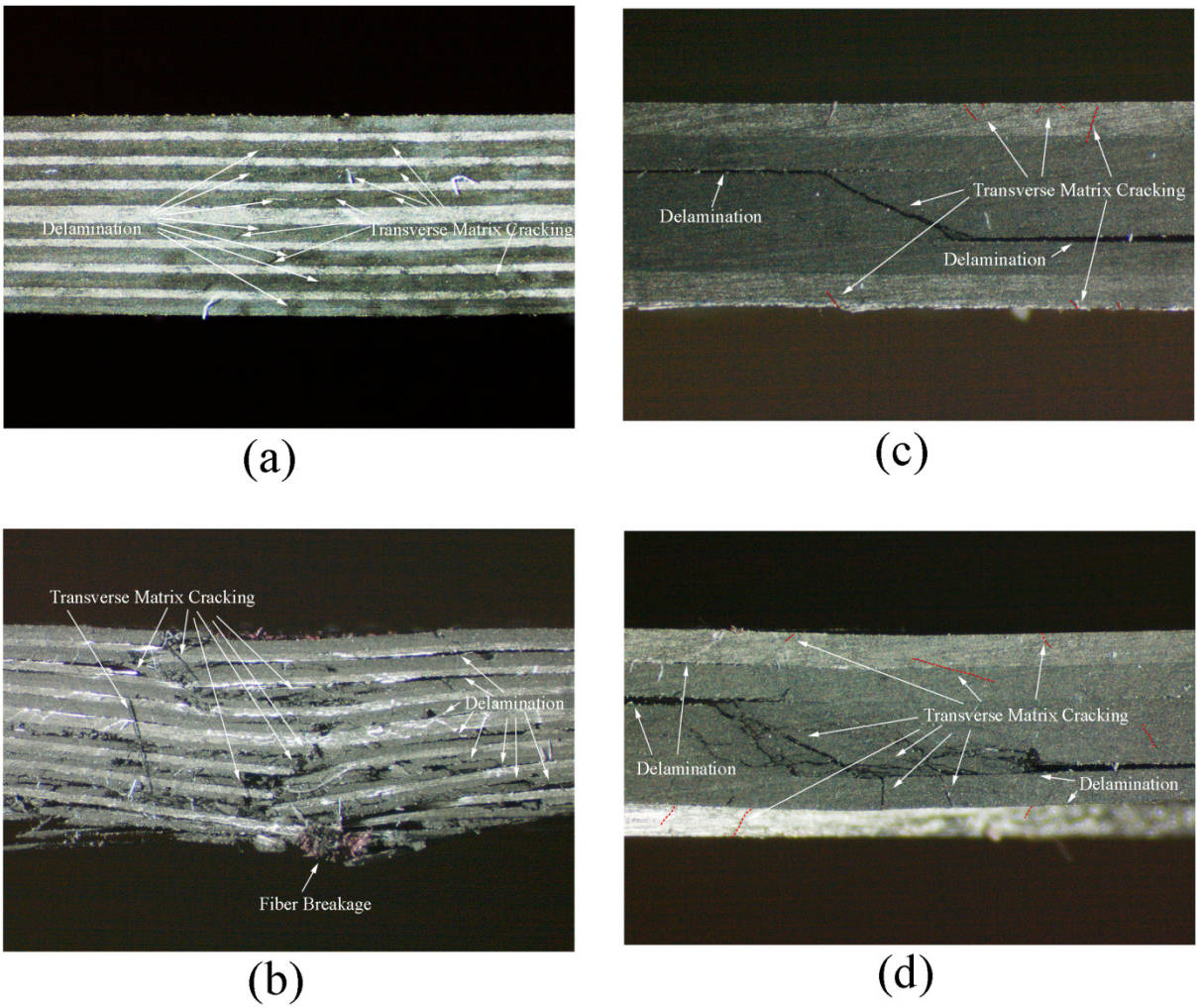

Fig. 5. A cross-section overview of midplane of the longitudinal direction for a) S_D-point 2, b) S_D-point 3, c) S_B-point 2, d) S_B-point 3.

Table 4. The area of the delamination region for the specimens.

Specimen	Load level	Delamination area (mm^2)
S_D	Point 2	135.6
	Point 3	556.5
S_B	Point 2	615.2
	Point 3	3847.4

4.2. AE-based study of damage mechanisms

Load and cumulative AE absolute energy versus displacement curves of the specimens are presented in Fig. 6. The AE activity of specimen S_B initiates earlier than specimen S_D. The first

significant damage in the specimens is well defined by a jump in the cumulative AE energy curve. The total AE energy of specimen S_B is about 7 times of the total AE energy of specimen S_D that it shows the occurrence of more damages in this specimen.

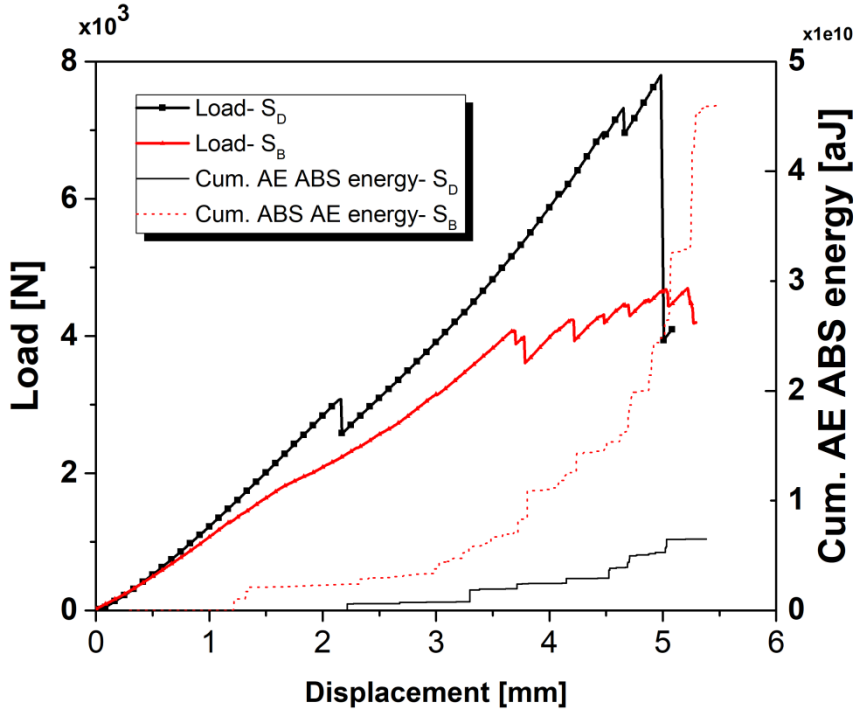

Fig. 6. Load and cumulative AE absolute energy versus displacement curves of the specimens.

One of the appropriate tools for characterization of damage evolution in composite materials which was utilized in literature, is the sentry function. The sentry function is defined as the logarithm of mechanical energy introduced to the structure/specimen to AE energy due to damage [46]:

$$f(x) = \mathrm{Ln}[\frac{E_s(x)}{E_a(x)}] \quad (15)$$

where $E_S(x)$, $E_a(x)$ and x are the mechanical energy (area beneath the load-displacement curve), the cumulative AE events energy and the displacement, respectively.

According to the state of the damage in the material, it may show four different trends as follows (see Fig. 7): S1: increasing trend; that shows there is no any considerable damage in the material. S2: suddenly drop; which shows that a considerable damage has been occurred in the material. S3: gradually decreasing; which illustrates the material is losing its load carrying capability. S4: constant trend; which shows that there is a balance between the occurrence of damages and some stiffening phenomena such as fiber bridging in the material.

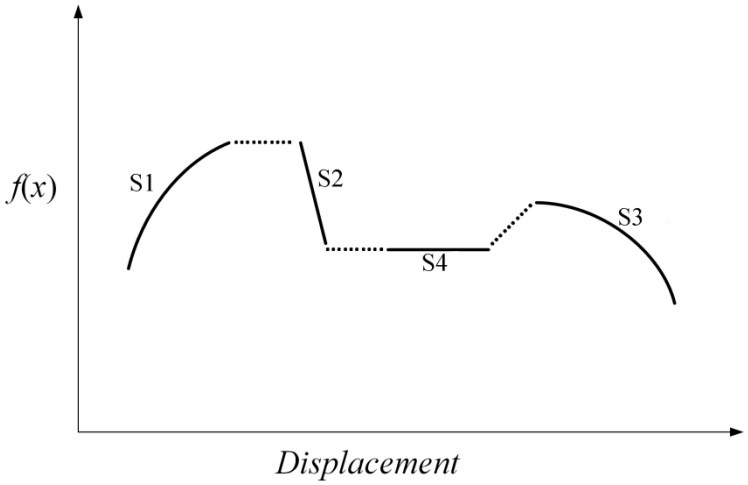

Fig. 7. The different trends of sentry function.

Fig. 8 shows sentry function curve of the specimens. For both specimens, there is an increasing trend (S1) at the end of the elastic region. Some oscillations and slope reduction in $S1_1$ may be due to the infinitesimal matrix cracking. Because matrix cracking cannot considerably degrade the stiffness of the structure individually, it usually does not lead to S2 type of the sentry function. The first S1, $S1_1$, is then followed by a sudden drop ($S2_1$) which is due to delamination. After this point, the sentry function behavior of specimen S_D can be explained by some S1 type trends that each of them is followed by one S2 trend. However, the slope of S1 trends gradually decreases due to the accumulation of damages and reducing the load carrying capability of the material with load

proceeding. The sentry function of specimen S_B has a similar trend with specimen S_D with this difference that after two increasing and suddenly drop trends, two constant trends are observed which is followed by a gradually decreasing of the sentry function ($S3_1$) that shows the specimen is losing its load carrying capability. Thus, sentry function shows that specimen S_B is lost its load carrying capability earlier than specimen S_D.

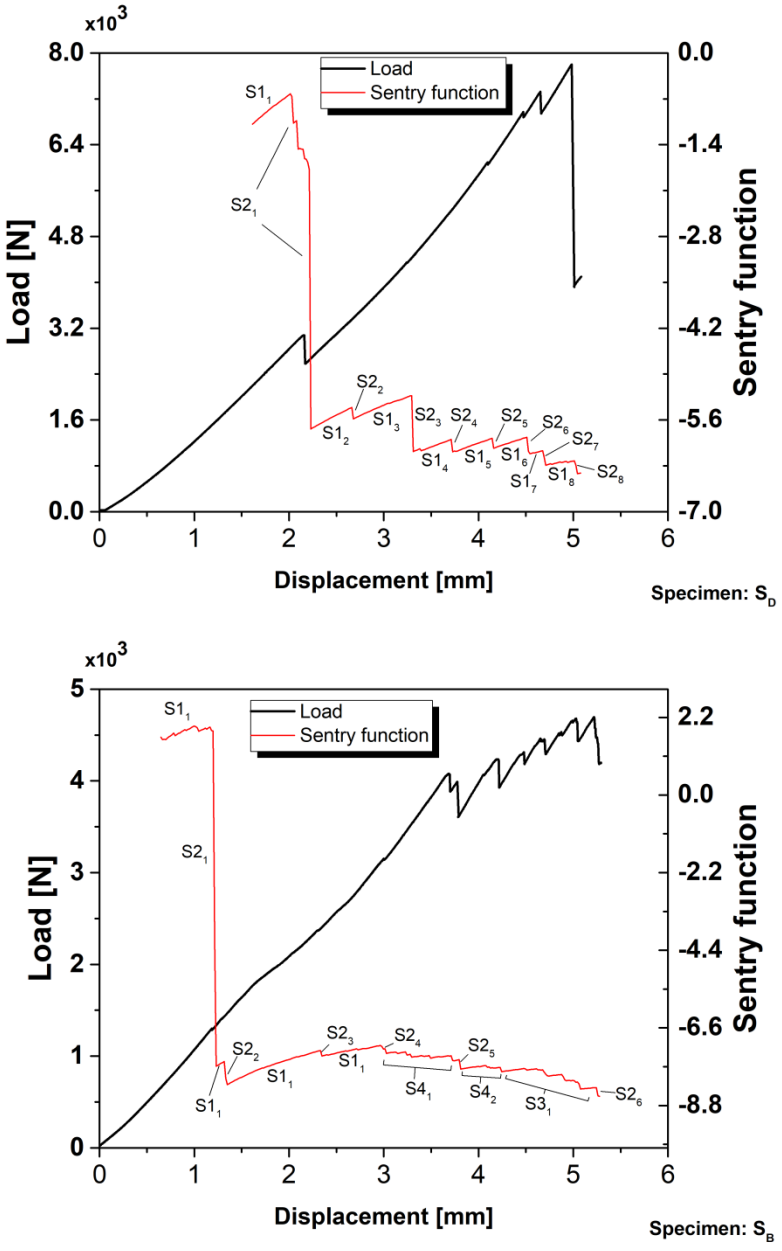

Fig. 8. The sentry function of the specimens.

4.3. Damage classification by AE

In order to characterize the induced damages at various load levels, the AE signals of different damages should be differentiated and be classified. Many researchers have used different clustering methods to classify AE signals of damaged composite laminates. However, they did not perform a thorough study about the limitation and repeatability of the utilized clustering methods. Thus, in order to establish a reliable SHM system based on AE, it is necessary to compare the performance of different clustering methods to classify AE signals. To this aim, six different clustering methods that mostly have been used in literature containing k-Means, Genetic k-Means, FCM, SOM, GMM, and hierarchical model are utilized to cluster AE signals of specimens S_D and S_B. Prior to clustering, the optimum number of clusters should be specified. To this aim, four criteria consisting of Calinski-Harabasz [47], Silhouette [48], Gap [41], and Davies-Bouldin [49] were utilized to specify the optimum clusters number. These methods do an iterative procedure to find the optimum clusters number, but their performances are a little different. The Calinski-Harabasz criterion is based on a ratio of the between-cluster variance to the within-cluster variance. The best solution has the largest between-cluster variance and the smallest within-cluster variance. The silhouette criterion measures the similarity of one point with its own cluster. The values of silhouette criterion are varied from -1 to +1 and the highest value of silhouette criterion shows that the point has a good similarity to its own cluster and is poorly matched to other clusters. The Gap criterion analyzes the change in within-cluster dispersion with the expected value of this parameter for the reference distribution. The highest value of Gap criterion illustrates the optimum solution. The Davies-Bouldin criterion is opposite to the Calinski-Harabasz criterion and it is defined as the ratio of within-cluster to between-cluster distances. Thus, the lowest value of Davies-Bouldin criterion shows the best clusters number. Thus, the highest value of Calinski-Harabasz, Silhouette, and Gap indices and the lowest value of Davies-Bouldin index show the best clusters number. Fig.

9 represents the values of these indices for the specimens. For specimen S_D, the best clusters number according to Calinski-Harabasz, Silhouette, and Gap criteria is 3 while Davies-Bouldin offers 2 as the optimum clusters number. Because most of the criteria suggest 3 clusters and also Davies-Bouldin index for 3 clusters is near to the index of 2 clusters, thus the optimum clusters number is considered 3. In the case of specimen S_B, Silhouette, Gap, and Davies-Bouldin criteria suggest 3 classes and Calinski-Harabasz suggests 6 classes. Because the Calinski-Harabasz index for 3 clusters is near to index for 6 clusters and also most of the criteria suggest 3, thus the optimum clusters number is considered 3.

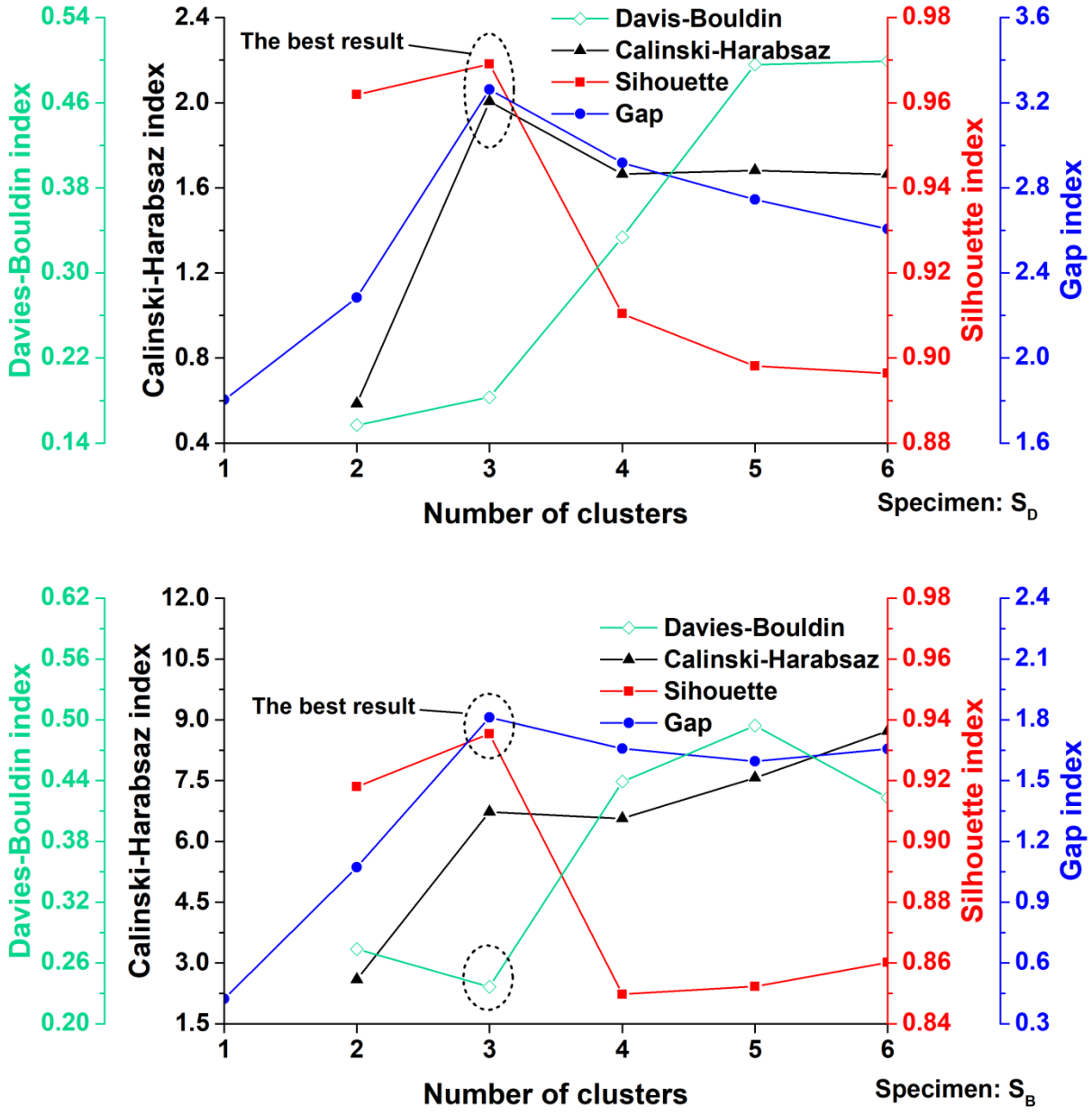

Fig. 9. The optimum clusters number for AE signals of specimens S_D and S_B.

According to literature review, the best parameters for AE signals clustering in composite materials are frequency and amplitude [21-23]. Thus these two parameters are selected as the features of the AE signals. Then, AE signals of specimens S_D and S_B are classified using the clustering methods. Fig. 10 shows the clustered AE signals of specimen S_D by different clustering methods. As can be seen, Genetic k-Means, FCM, SOM, and hierarchical methods partitioned data

into three classes with frequency ranges [50-150 kHz], [150-400 kHz], and above 400 kHz, which has a good consistency with the data appearance. While, k-Means method divides the first partition, [50-150 kHz], into two clusters and combines two next clusters, i.e. [150-400 kHz] and above 400 kHz. In addition, GMM method partitions two first clusters in a wrong manner. This fault is due to the fact that the performance of k-Means clustering depends on the initial randomly selected cluster centroids and there is no guarantee that the algorithm converges to the optimum solution every times [23, 38]. Also, the performance of GMM depends on the initially selected Gaussian parameters and they may be changed during each iteration [42].

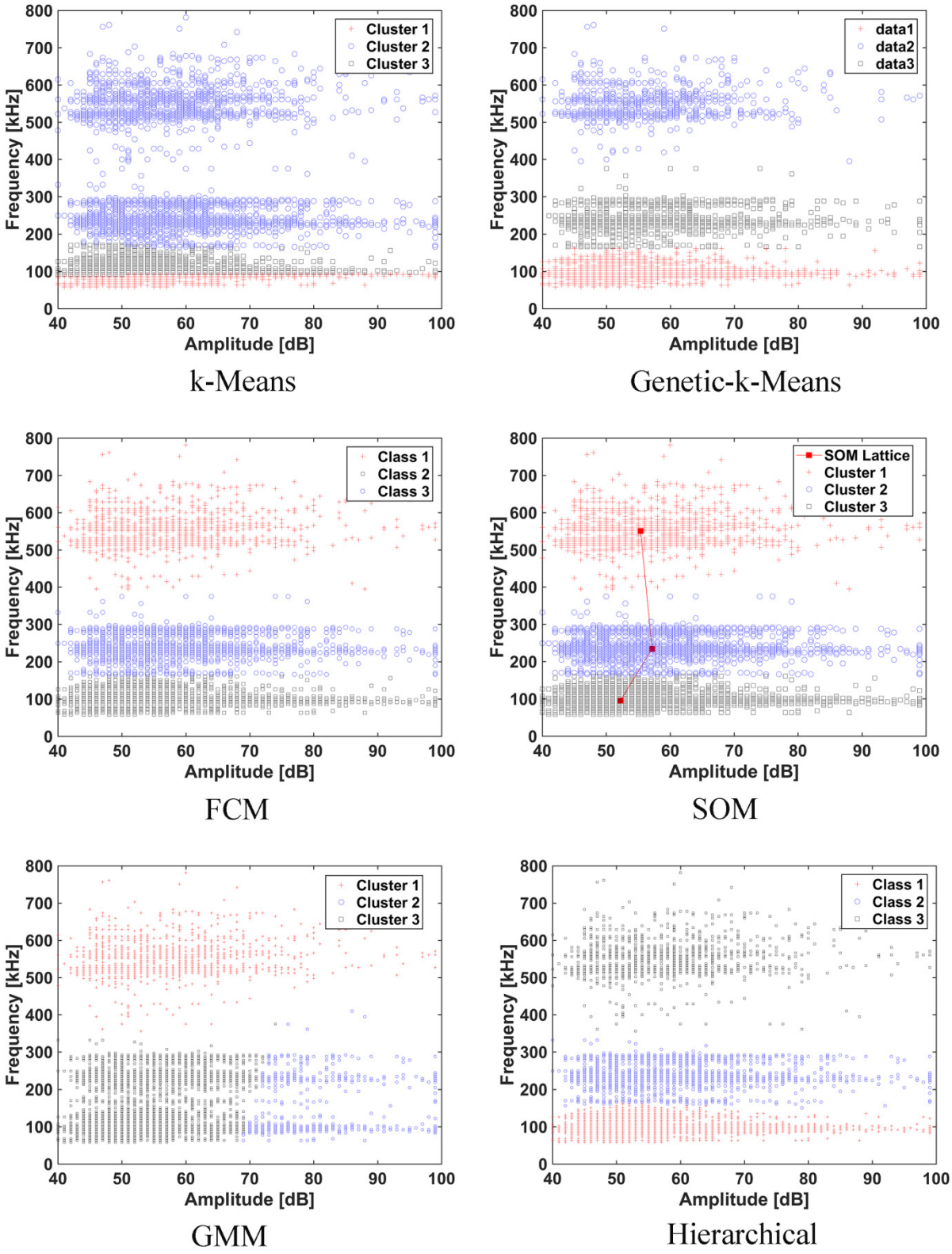

Fig. 10. The functionality of the different clustering methods for clustering AE signals of specimen S_D.

The aim is selecting the best clustering method among Genetic k-Means, FCM, SOM, and hierarchical methods. Most of the clustering methods get stuck in local minima when there are some dense regions in the space of data, where huge amount of data aggregate there. In order to examine the performance of the clustering methods in this situation, one artificial cluster with the frequency range of [0-50 kHz] is added to the AE signals of specimen S_D. To create this artificial cluster, the cluster with the frequency range of [50-150 kHz] is copied and the number of its data is increased to three times by duplication of data in this cluster. The best clusters number which was evaluated for the new data set is 4. In order to ensure the repeatability of the results of the clustering methods, the clustering process is repeated several times for each clustering method. Fig. 11 shows the results of different clustering methods for the new AE data. As can be seen, SOM method detects the artificial cluster in all iterations but it does not classify other AE data correctly. For example, it combines a part of signals with the frequency less than 300 kHz with the signals that have the frequency higher than 500 kHz. This is due to the fact that because of defining a neighborhood function between lattice neurons, most of the lattice neurons usually aggregate in the dense regions of the data [41]. Thus, because a considerable number of AE data has been located in the frequency range of [0-50 kHz], therefore neurons try to aggregate in this region. Although FCM and Genetic k-Means could classify the data appropriately, but their results do not have repeatability for the next iterations. Therefore, although the combination of Genetic and Fuzzy methods with k-Means clustering could considerably improve the performance of this method, however, they do not still have a unique result at each iteration for more complicated situations. Thus, these methods are not reliable methods to be used in a SHM system. Finally, the only method which gives a unique optimum result at each iteration is hierarchical model clustering. Due to the top-down structure of hierarchical clustering method, it does not get stuck in local

minima and gives a unique result at each iteration [43]. Thus, hierarchical model clustering is utilized for the final clustering of AE signals of specimens S_D and S_B.

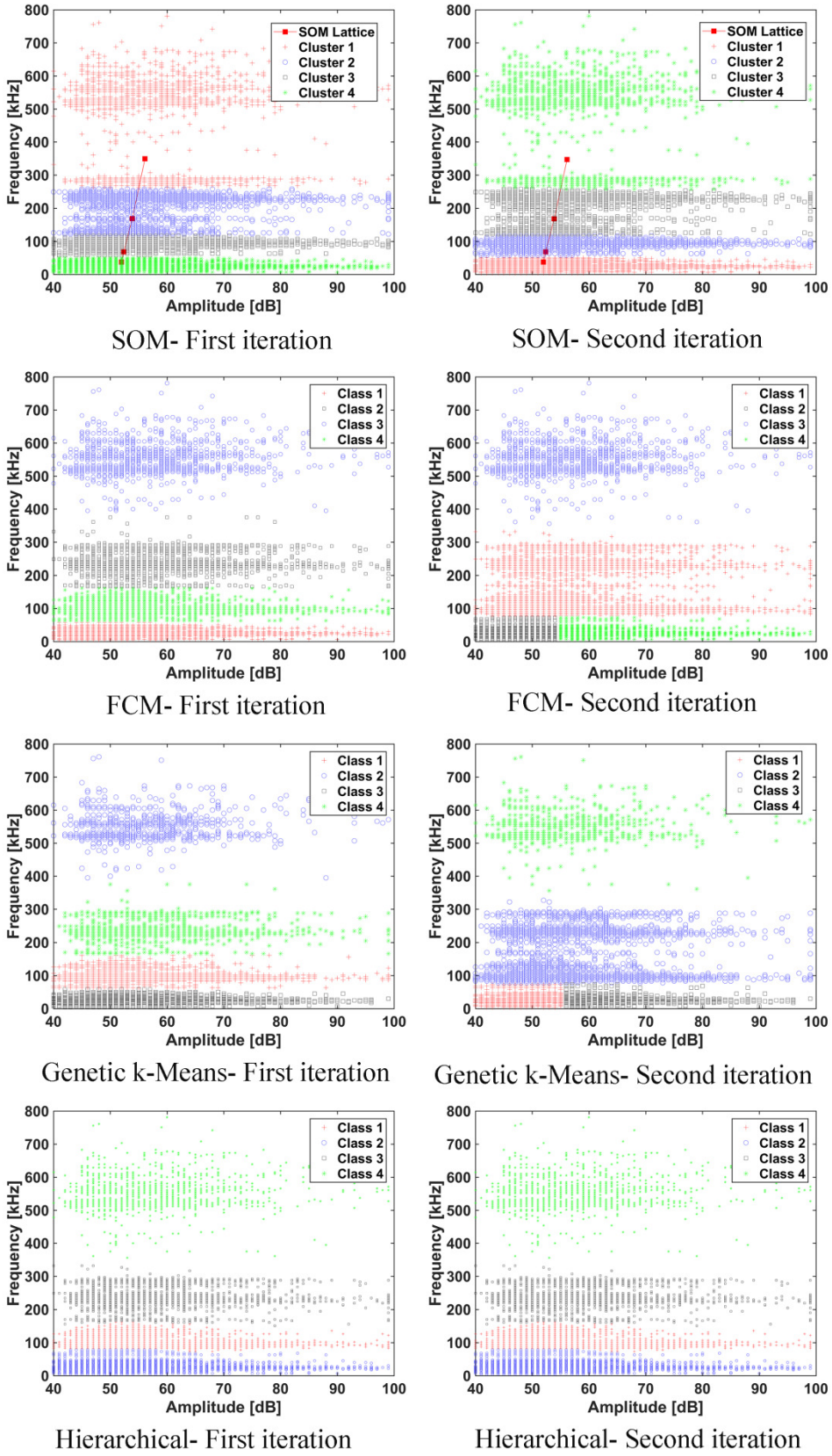

Fig. 11. The performance of the different clustering methods for clustering of the artificial AE signals.

Fig. 12 shows the clustered AE data for specimens S_D and S_B by hierarchical model. The next step is assigning these clusters to the interlaminar and intralaminar damage mechanisms. Fig. 13 shows the reported frequency ranges in literature for different damage mechanisms in carbon/ epoxy laminated composites under different loading conditions. All of these damages usually do not occur simultaneously and only some of these damages may occur in the material depending on the loading conditions. For example, Boominathan et al. [31] reported the occurrence of three damage mechanisms in carbon laminated composites under low-velocity impact, consisting of matrix cracking, fiber failure, and delamination which are in accordance with the observed damages in specimens S_D and S_B. Although there are considerable differences between the reported frequency range of different damage mechanisms in literature (see Fig. 13), however, most of the researchers reported that matrix cracking has the lowest frequency content, fiber failure has the highest frequency, and the frequency of delamination signals is located between these two damages [31, 50, 53]. Therefore, the clusters in Fig. 12 are dedicated to these three damage mechanisms as follows: Cluster 1 which has the lowest frequency content is dedicated to matrix cracking, cluster 3 with the highest frequency content is devoted to fiber failure, and cluster 2 with the frequency content between these clusters is allocated to delamination.

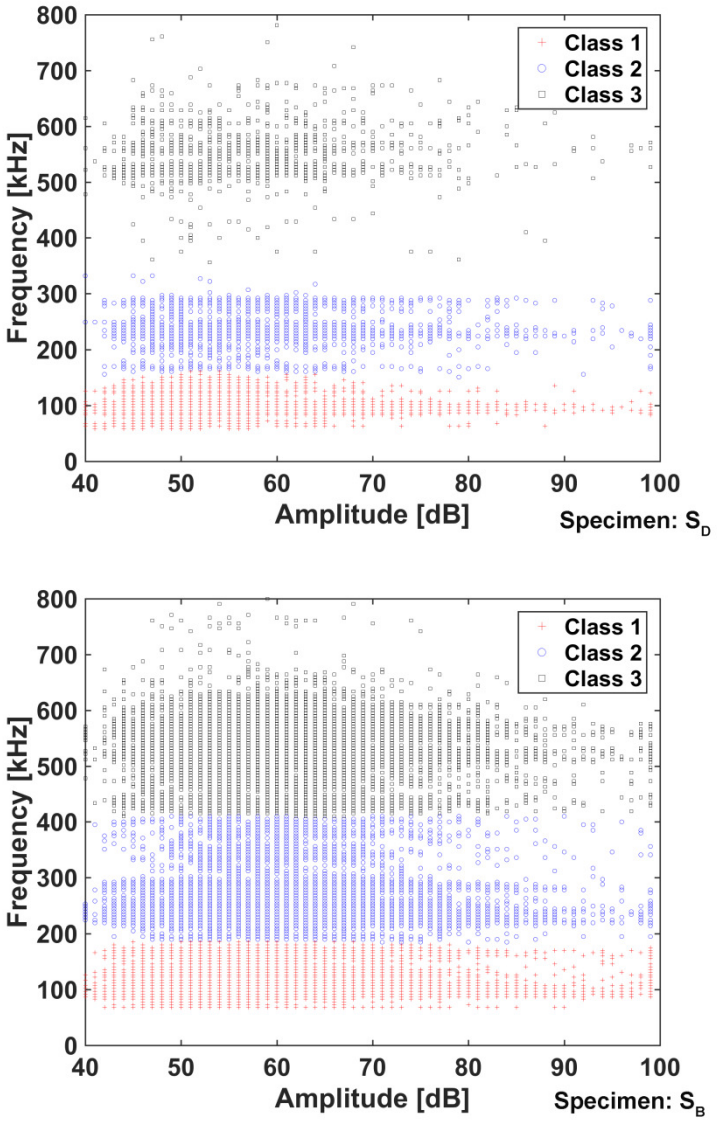

Fig. 12. The clustering of the AE signals of specimens S_D and S_B using hierarchical method.

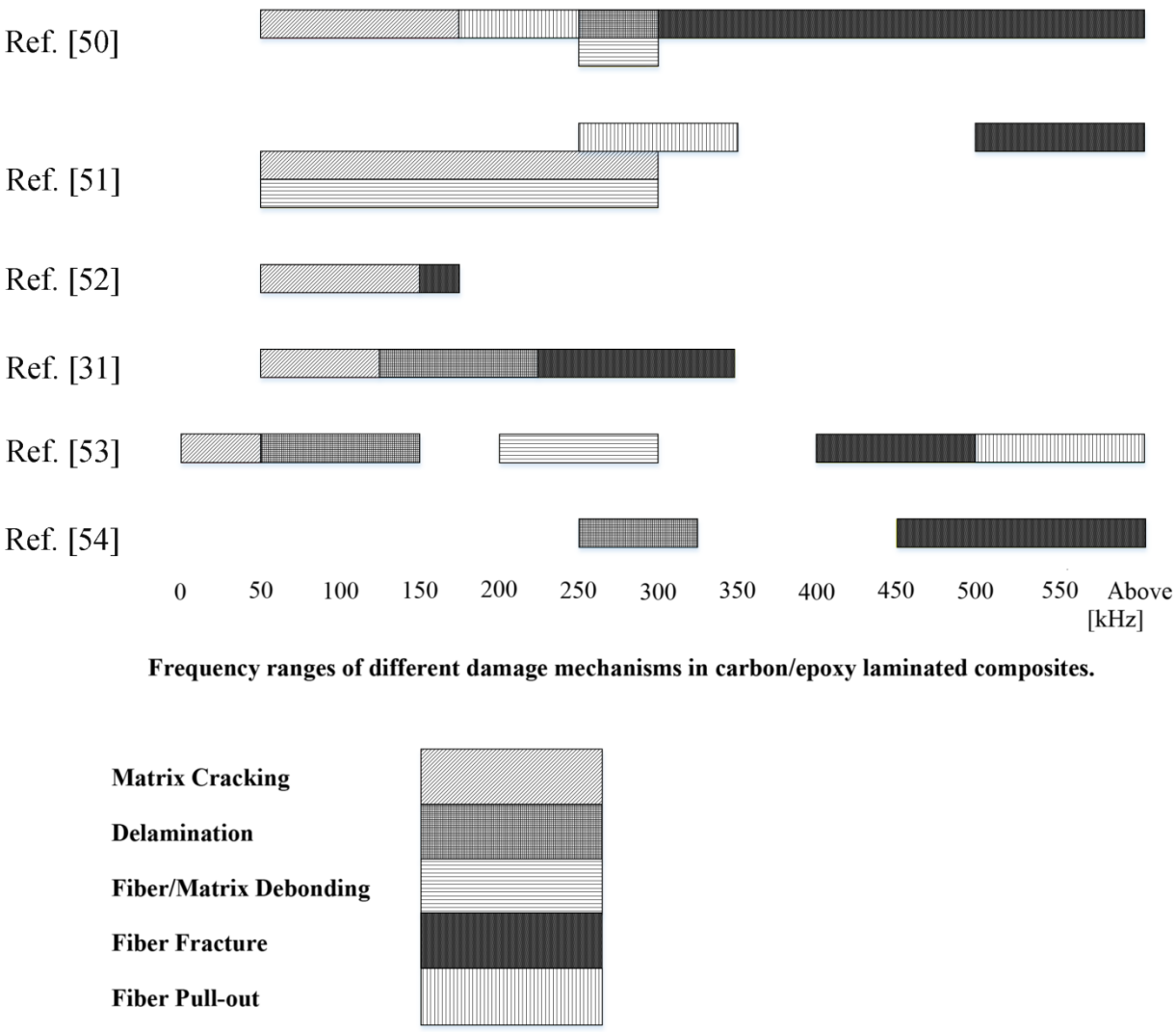

Fig. 13. The frequency content reported in literature for different damage mechanisms in carbon/epoxy laminated composites under different loading conditions.

The cumulative number of AE events for each cluster was calculated and it is shown in Fig. 14. As can be seen, for specimen S_D, matrix cracking signals initiate a little before the first load drop which has a good consistency with the observed first matrix cracking at point 1 of Fig. 3, while the delamination and fiber failure signals initiate after matrix cracking, at the moment of the first load drop. In the case of specimen S_B, matrix cracking and fiber failure start a little before the nonlinearity point and delamination initiates a little after them. Also, the total number of damage's

AE events for specimen S_B is much higher than specimen S_D (about 5 times) that it shows the damage of specimen S_B is more than specimen S_D. This is consistent with the fact that the load carrying capacity of specimen S_B is less than specimen S_D (see Fig. 2). Also, as it was mentioned previously, the dominant loading mode of specimen S_D is penetration, thus most of damages occur in a small region around the loading point, while the dominant loading mode of specimen S_B is bending that leads to increasing the area that is susceptible to damage.

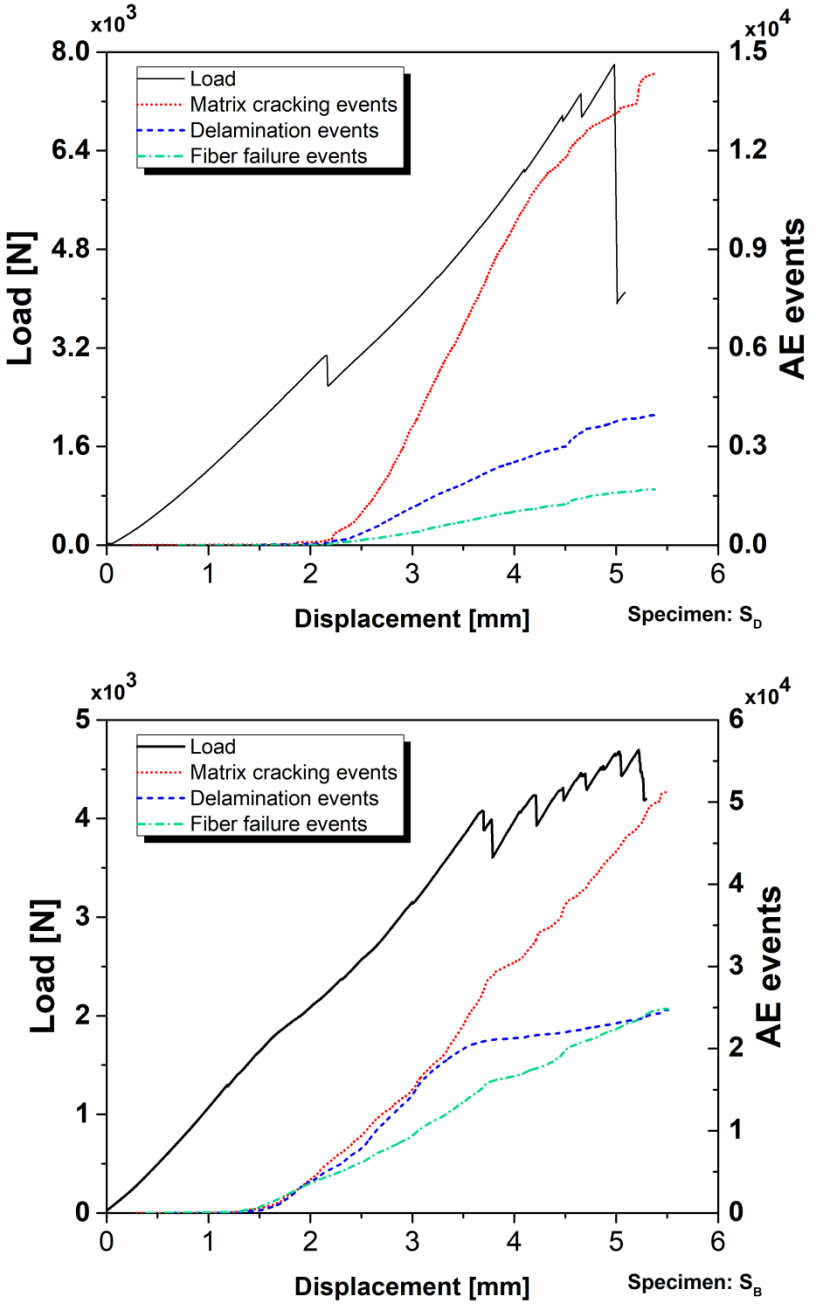

Fig. 14. The AE events of different damage mechanisms of specimens S_D and S_B.

The number of events is not an appropriate parameter to characterize damages in the specimens, because an event does not offer any information about the intensity of the corresponded damage. For example, both an infinitesimal delamination growth and a big delamination growth introduce

one event, while the energy content of the event of the big delamination growth is much higher than the event of the infinitesimal delamination growth. Thus, in order to compare the behavior of different damage mechanisms, the cumulative AE energy of the AE events is calculated. Fig. 15 illustrates the cumulative AE energy of the damage mechanisms in the specimens. The cumulative AE energy curves of specimen S_D have an unstable behavior (jumping behavior) while the curves of specimen S_B are smoother. Although matrix cracking signals initiates before the first load drop in specimen S_D, but the energy content of these signals is not considerable until displacement 2.5 mm, while, the energy of delamination signals at the first load drop is considerable. This is due to occurring of many delaminations at this point in specimen S_D. The energy of fiber failure signals also starts increasing after other damage mechanisms. The unstable behavior of cumulative AE energy curves of specimen S_D is due to inducing new delamination at different interfaces with the load proceeding. In the case of specimen S_B, because the number of induced delamination at the end of linear region is low, thus there is not a significant jump in cumulative AE energy curve of delamination at this point, while matrix cracking shows a jump at there. Fiber failure is also the last mechanism that activates in this specimen.

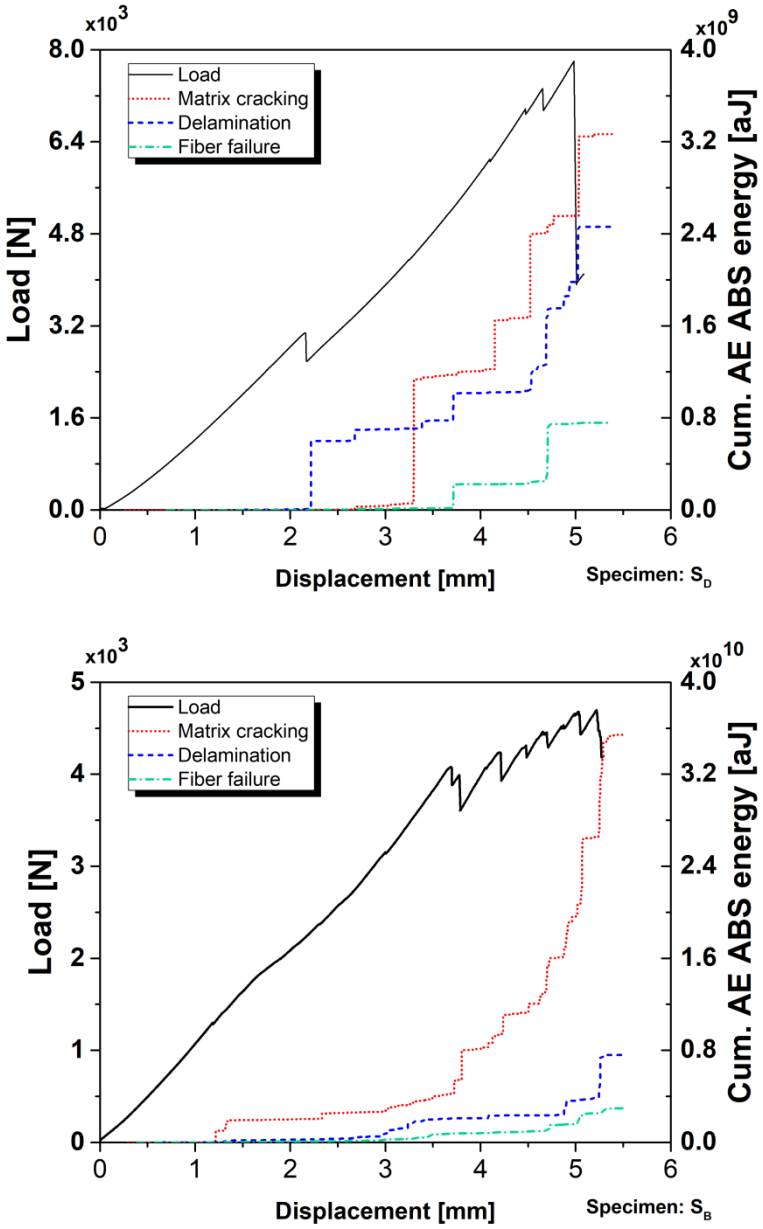

Fig 15. The cumulative AE energy curves of damage mechanisms for specimens S_D and S_B.

Table 5 represents the number of events and cumulative AE energy of each damage mechanisms for the specimens. The total number of events and cumulative AE energy of specimen S_B are 5 and 7 times of specimen S_D, respectively. It shows that amount of the damages in specimen S_B is higher than specimen S_D. Comparing of the load carrying capacity of the specimens (see Fig. 2) also confirms this claim.

As been mentioned above, to characterize the state of damages in the specimens, cumulative AE energy is a better parameter in comparing with the number of AE events. The dominant damage mechanism in both specimens is matrix cracking with 50.3% and 77.1% of AE energy of damage's signals for specimens S_D and S_B, respectively. The second damage mechanism in the specimens is delamination. The percentage of delamination in specimen S_D (38.0%) is higher than specimen S_B (16.5%). The lower value of matrix cracking percentage and higher value of delamination percentage in specimen S_D is due to the higher number of dissimilar interfaces that susceptible to delamination in S_D. Thus, amount of matrix cracking reduces while delamination increases in this specimen. Also, the higher percentage of fiber failure in specimen S_D refers to the penetration of indenter through the specimen S_D that leads to fiber fracture at the back face of this specimen (see Figs. 3 and 5).

Table 5. The value of AE events and cumulative AE energy of the damage mechanisms.

Specimen		Damage mechanisms			Total
		Matrix cracking	Delamination	Fiber failure	
S_D	Events number	14,352 71.7%	3,960 19.8%	1,698 8.5%	20,010 100%
	Cum. AE energy (aJ)	3.26e9 50.3%	2.46e9 38.0%	7.57e8 11.7%	6.48e9 100%
S_B	Events number	51,245 50.8%	24,699 24.5%	24,842 24.7%	100,785 100%
	Cum. AE energy (aJ)	3.54e10 77.1%	7.59e9 16.5%	2.94e9 6.4%	4.59e10 100%

5. Conclusion

This study was devoted to the clustering of the indentation-induced interlaminar and intralaminar damages in carbon/epoxy laminated composites using AE technique. To this aim, two quasi-isotropic carbon/epoxy laminated composites with dispersed ($[60/0/-60]_{4S}$) and blocked

($[60_4/0_4/-60_4]_{S)}$ layups were fabricated and subjected to a quasi-static indentation loading. First, the load-displacement curve and the digital camera and ultrasonic C-scan images used to study the intralaminar and interlaminar damages of the specimens. The results showed the load carrying capability of dispersed specimen is 1.7 times of blocked specimen and also the area of delaminated region for this specimen is 0.14 times of the delaminated area for blocked specimen. However, the number of delaminated interfaces for the dispersed specimen is higher than the blocked specimen (22 delaminated interfaces for S_D against 4 delaminated interfaces for S_B). Then, the AE signals were clustered to identify different damage mechanisms in the specimens. In order to select the best clustering method, the performance of six different clustering methods consisting of k-Means, Genetic k-Means, FCM, SOM, GMM, and hierarchical model were compared. The results showed that the best clustering method which has a reliable and repeatable performance is hierarchical model. Thus, the AE signals of the specimens were clustered by hierarchical model and the evolution behavior of different damage mechanisms during loading was studied. The obtained results show that the combination of AE technique with an appropriate clustering method such as hierarchical model can be a valuable tool for structural health monitoring of composite structures.

References

[1] Zhang J, Zhang X. Simulating low-velocity impact induced delamination in composites by a quasi-static load model with surface-based cohesive contact. Compos Struct 2015; 125: 51–7.

[2] Senthilnathan K, Hiremath CP, Naik NK, Guha A, Tewari A. Microstructural damage dependent stiffness prediction of unidirectional CFRP composite under cyclic loading. Composites Part A 2017; 100: 118-27.

[3] Salvetti M, Sbarufatti C, Gilioli A, Dziendzikowski M, Dragan K, Manes A, Giglio M. On the mechanical response of CFRP composite with embedded optical fibre when subjected to low velocity impact and CAI tests. Compos Struct 2017; 179: 21-34.

[4] Tan W, Falzon BG, Chiu LNS, Price M. Predicting low velocity impact damage and Compression-After-Impact (CAI) behaviour of composite laminates. Composites Part A 2015; 71: 212–26.

[5] Liu PF, Liao BB, Jia LY, Peng XQ. Finite element analysis of dynamic progressive failure of carbon fiber composite laminates under low velocity impact. Compos Struct 2016; 149: 408-22.

[6] Jung KH, Kim DH, Kim HJ, Park SH, Jhang KY, Kim HS. Finite element analysis of a low-velocity impact test for glass fiber-reinforced polypropylene composites considering mixed-mode interlaminar fracture toughness. Compos Struct 2017; 160: 446–56.

[7] Li N, Chen PH. Micro–macro FE modeling of damage evolution in laminated composite plates subjected to low velocity impact. Compos Struct 2016; 147: 111–21.

[8] Diamanti K, Soutis C. Structural health monitoring techniques for aircraft composite structures. Prog Aerosp Sci 2010; 46(8): 342-52.

[9] Wymore ML, Van Dam JE, Ceylan H, Qiao D. A survey of health monitoring systems for wind turbines. Renewable Sustainable Energy Rev 2015; 52: 976–90.

[10] Li Y, Yang ZW, Zhu JT, Ming AB, Zhang W, Zhang JY. Investigation on the damage evolution in the impacted composite material based on active infrared thermography. NDT and E Int 2016; 83: 114-22.

[11] Castellano A, Fraddosio A, Piccioni MD. Ultrasonic goniometric immersion tests for the characterization of fatigue post-LVI damage induced anisotropy superimposed to the constitutive anisotropy of polymer composites. Composites Part B 2017; 116: 122-36.

[12] Jespersen KM, Zangenberg J, Lowe T, Withers PJ, Mikkelsen LP. Fatigue damage assessment of uni-directional non-crimp fabric reinforced polyester composite using X-ray computed tomography. Compos Sci Technol 2016; 136: 94-103.

[13] Saeedifar S, Fotouhi M, Ahmadi Najafabadi M, Hossein Hosseini Toudeshky H, Minak G. Prediction of quasi-static delamination onset and growth in laminated composites by acoustic emission. Composites Part B 2016; 85: 113-22.

[14] Mohammadi R, Saeedifar M, Hosseini Toudeshky H, Ahmadi Najafabadi M, Fotouhi M. Prediction of delamination growth in carbon/epoxy composites using a novel acoustic emission-based approach. J Reinf Plast Compos 2015; 34(11): 868-78.

[15] Fallahi N, Nardoni G, Heidary H, Palazzetti R, Yan X, Zucchelli A. Supervised and non-supervised AE data classification of nanomodified CFRP during DCB tests, FME Trans 2016; 44(4): 415-21.

[16] Yousefi J, Mohamadi R, saeedifar M, Ahmadi M, Toudeshky H. Delamination characterization in composite laminates using acoustic emission features, micro visualization and finite element modeling. J Compos Mater 2015; DOI: 10.1177/0021998315615691.

[17] Loutas T, Eleftheroglou N, Zarouchas D. A data-driven probabilistic framework towards the in-situ prognostics of fatigue life of composites based on acoustic emission data. Compos Struct 2017; 161: 522-9.

[18] Zarouchas D, Hemelrijck D. Mechanical characterization and damage assessment of thick adhesives for wind turbine blades using acoustic emission and digital image correlation techniques. J Adhes Sci Technol 2014; 28(14-15): 1500-16.

[19] Miller RK. Nondestructive testing handbook: acoustic emission testing. 5th ed. American Society for Nondestructive Testing; 1987.

[20] Ai SP, Xu CH, Chen GM, Li GR. Acoustic emission monitoring of degradation in plain weave CFRP composite laminate. AASRI International Conference on Industrial Electronics and Applications 2015; 63-6.

[21] Fotouhi M, Heidary H, Ahmadi M, Pashmforoush F. Characterization of composite materials damage under quasi-static three-point bending test using wavelet and fuzzy C-means clustering. J Compos Mater 2012; 46(15): 1795-808.

[22] Pashmforoush F, Fotouhi M, Mehdi Ahmadi M. Damage characterization of glass/epoxy composite under three-point bending test using acoustic emission technique. J Mater Eng Perform 2012; 21(7): 1380–90.

[23] Pashmforoush F, Khamedi R, Fotouhi M, Hajikhani M, Ahmadi M. Damage classification of sandwich composites using acoustic emission technique and k-means genetic algorithm. J Nondestr Eval 2014; 33 (4): 481-92.

[24] Abir MR, Tay TE, Ridha M, Lee HP. Modelling damage growth in composites subjected to impact and compression after impact. Compos Struct 2017; 168: 13-25.

[25] Singh H, Namala KK, Mahajan P. A damage evolution study of E-glass/epoxy composite under low velocity impact. Composites Part B 2015; 76: 235-48.

[26] Jung KH, Kim DH, Kim HJ, Park SH, Jhang KY, Kim HS. Finite element analysis of a low-velocity impact test for glass fiber-reinforced polypropylene composites considering mixed-mode interlaminar fracture toughness. Compos Struct 2017; 160: 446–56.

[27] Aymerich F, Dore F, Priolo P. Simulation of multiple delaminations in impacted cross-ply laminates using a finite element model based on cohesive interface elements. Compos Sci Technol 2009; 69: 1699–709.

[28] Singh H, Mahajan P. Analytical modeling of low velocity large mass impact on composite plate including damage evolution. Compos Struct 2016; 149: 79-92.

[29] Panettieri E, Fanteria D, Montemurro M, Froustey C. Low-velocity impact tests on carbon/epoxy composite laminates: A benchmark study. Composites Part B 2016; 107: 9-21.

[30] Suresh Kumar C, Arumugam V, Santulli C. Characterization of indentation damage resistance of hybrid composite laminates using acoustic emission monitoring. Composites Part B 2017; 111: 165-178.

[31] Boominathan R, Arumugam V, Santulli C, Adhithya Plato Sidharth A, Anand Sankar R, Sridhar BTN. Acoustic emission characterization of the temperature effect on falling weight impact damage in carbon/epoxy laminates. Composites Part B 2014; 56: 591–8.

[32] Mahdian A, Yousefi J, Nazmdar M, Zarif Karimi N, Ahmadi M, Minak G. Damage evaluation of laminated composites under low-velocity impact tests using acoustic emission method. J Compos Mater 2017; 51(4): 479-90.

[33] Petrucci R, Santulli C, Puglia D, Nisini E, Sarasini F, Tirillò J, Torre L, G. Minak G, Kenny JM. Impact and post-impact damage characterisation of hybrid composite laminates based on basalt fibres in combination with flax, hemp and glass fibres manufactured by vacuum infusion. Composites Part B 2015; 69: 507–15.

[34] Hexcel Product Data. HexPly® 8552 Epoxy matrix (180°C/356°F curing matrix). Hexcel Composites Publication, FTA 072e, 2013.

[35] Marlett K. Hexcel 8552 IM7 unidirectional prepregs 190 gsm & 35%RC qualification material property data report. CAM-RP-2009-015, National Institute for Aviation Reserach, 2011.

[36] ASTM E976–10. Standard guide for determining the reproducibility of acoustic emission sensor response. West Conshohocken, PA: ASTM International, 2010.

[37] Hartigan JA, Wong MA. A K-means clustering algorithm. J Royal Stat Soc C 1979;28(1):100–8.

[38] Jain AK. Data clustering: 50 years beyond K-means. Pattern Recognit Lett 2010; 31(8): 651-66.

[39] Bezdek JC, Ehrlich R, Full W. FCM: The fuzzy c-means clustering algorithm. Comput Geosci 1984; 10(2–3): 191-203.

[40] Bhattacharyya S, Pan I, Mukherjee A, Dutta P. Hybrid intelligence for image analysis and understanding. John Wiley & Sons Ltd, 2017; 9-10.

[41] Vesanto J, Alhoniemi E. Clustering of the Self-Organizing Map. IEEE Trans Neural Networks 2000; 11(3): 586-600.

[42] Bishop CM. Pattern Recognition and Machine Learning. Springer Science+Business Media, Singapore, 2006; 430-55.

[43] Murtagh F. A survey of recent advances in hierarchical clustering algorithms. Comput J 1983; 26(4): 354–9.

[44] Hollaway L. Polymers and polymer composites in construction. London; Thomas Telford Ltd.: 1990, 52-55.

[45] Heracovich CT. Mechanics of fibrous composites. John Wiley & Sons, USA, 1998: 255-8.

[46] Refahi Oskouei A, Zucchelli A, Ahmadi M, Minak G. An integrated approach based on acoustic emission and mechanical information to evaluate the delamination fracture toughness at mode I in composite laminate. Mater Des 2011; 32(3): 1444-55.

[47] Calinski RB, Harabasz J, A dendrite method for cluster analysis. Comm in Statistics 1974; 3: 1-27.

[48] Rousseeuw P. Silhouettes: a graphical aid to the interpretation and validation of cluster Analysis. J Comput Appl Math 1987; 20: 53-65.

[49] Davies DL, Bouldin DW .A Cluster separation measure. IEEE Trans Pattern Anal Mach Intell 1979; 1: 224-7.

[50] De Groot PJ, Wijnen PAM, Janssen RBF. Real-time frequency determination of acoustic emission for different fracture mechanisms in carbon/epoxy composites. Compos Sci Technol 1995; 55: 405-12.

[51] Komai K, Minoshima K, Shibutani T. Investigations of the fracture mechanism of carbon/epoxy composites by AE signal analyses. JSME Int J 1991; 34(3): 381-8.

[52] Russell SS, Henneke EG. Signature analysis of acoustic emission from graphite/epoxy composites. Interim report, NASA Grant NSG 1238, Report No. VPI-E-77-22, 1977.

[53] Gutkin R, Green CJ, Vangrattanachai S, Pinho ST, Robinson P, Curtis PT. On acoustic emission for failure investigation in CFRP: Pattern recognition and peak frequency analyses. Mech Syst Sig Process 2011; 25: 1393–407.

[54] Chou HY, Mouritz AP, Bannister MK, Bunsell AR. Acoustic emission analysis of composite pressure vessels under constant and cyclic pressure. Composites Part A 2015; 70: 111–20.

List of Figure captions

Fig. 1. a) The composite specimen, and b) the indentation test setup.

Fig. 2. The load-displacement curve of the specimens.

Fig. 3. The damages at the front and back faces of the specimens at different load levels.

Fig. 4. Delamination contours obtained from ultrasonic C-scan of a) S_D-point 2, b) S_D-point 3, c) S_B-point 2, d) S_B-point 3.

Fig. 5. A cross-section overview of midplane of the longitudinal direction for a) S_D-point 2, b) S_D-point 3, c) S_B-point 2, d) S_B-point 3.

List of Table captions